

## Surface-enhanced Raman scattering on dual-layer metallic grating structures

GUAN ZhiQiang<sup>1</sup>, HÅKANSON Ulf<sup>2</sup>, ANTTU Nicklas<sup>2</sup>, WEI Hong<sup>1</sup>, XU HongQi<sup>2</sup>,  
MONTELIUS Lars<sup>2</sup> & XU HongXing<sup>1,2\*</sup>

<sup>1</sup>Nanoscale Physics and Devices Laboratory, Institute of Physics, Chinese Academy of Sciences, Beijing 100190, China;

<sup>2</sup>Division of Solid State Physics/The Nanometer Structure Consortium, Lund University, Lund S-221 00, Sweden

Received December 21, 2009; accepted February 5, 2010

Dual-layer Metallic grating (DMG) structures as surface-enhanced Raman scattering (SERS) substrates are studied using benzenethiol as the probe analyte. The DMG structure consists of a SiO<sub>2</sub> grating and 100-nm-thick gold coating layers. An enhancement factor of 10<sup>5</sup> is achieved by optimizing the SiO<sub>2</sub> grating height within the range from 165 to 550 nm. The enhancement factor dependence on the SiO<sub>2</sub> grating height is due to the surface plasmon excitation, which is dependent on the polarization of the incident light, and confirmed by finite difference time domain simulations. This study demonstrates the advantages of high uniformity, reproducibility and sensitivity in the DMG structures for SERS applications.

**surface-enhanced Raman scattering, surface plasmon, dual-layer metallic grating**

**Citation:** Guan Z Q, Håkanson U, Anttu N, et al. Surface-enhanced Raman scattering on dual-layer metallic grating structures. Chinese Sci Bull, 2010, 55: 2643–2648, doi: 10.1007/s11434-010-3189-1

Surface-enhanced Raman scattering (SERS) has been widely studied in recent decades due to the high chemical specificity of vibrational spectra and increased detection efficiency by huge enhancement factors. It has been recognized that the origin of the enhancement in SERS is coming from electromagnetic (EM) and chemical components [1–3]. The EM enhancement coming from the excitation of surface plasmons (SPs) in noble or transition metals is usually several orders of magnitude higher than the chemical enhancement, and thus it is the main contributor to the SERS enhancement for most cases [4–7]. SPs are the collective oscillations of the electron gas in a metal. The excitation of SPs in metal nanostructures can produce an enhanced optical field, which is the physical basis for surface-enhanced spectroscopy, particularly for SERS. A volume where the electromagnetic field is strongly enhanced is usually called a “hot spot”. When the molecules are located in the “hot spots”, the Raman scattering intensity will be significantly

magnified, which largely improves the sensitivity of Raman detection even to a single molecule level [8,9]. The high sensitivity and fingerprint property make SERS a powerful technique for chemical- and bio-sensing applications [10–12]. Recently, SERS was employed in the diagnosis and therapy of diseases [13–15].

In the studies of SERS, different substrates have been developed, of which colloidal metal nanoparticles are widely used due to their large SERS enhancement and easy preparation. Single molecule SERS experiments were achieved in colloidal nanoparticle systems. In addition, the electromagnetic enhancement contribution to SERS was also first clearly elucidated from both experiment and theory in Ag nanoparticle aggregates [5,16], in which the gaps between the nanoparticles are “hot spots” for SERS due to the strong electromagnetic coupling between adjacent particles. However, the plasmonic coupling is often sensitive to the polarization of the excitation light, so the SERS intensity in metal nanostructures is usually polarization dependent [17,18]. Our recent work [6] showed that, in the total

\*Corresponding author (email: hxxu@aphy.iphy.ac.cn)

SERS enhancement, only the part originating from the enhancement of the electric field at the incident frequency depends on the incident polarization, while the enhancement originating from the electric field enhancement at the Raman frequency is determined by the nanostructures and is not dependent on the incident polarization. In addition to the field enhancement, metal nanoparticles can also serve as nanoantennas to control the emission polarization of the emitters residing in the nanoparticle junctions, which can be used to design a polarization rotator at the nanometer scale [19,20].

Although the nanoparticles can generate “hot spots” with very high SERS enhancement ( $>10^{10}$ ) [9,16], the reproducibility and the uniformity of the measurements is poor due to the small efficient volume and poor size and position control of the particles. Periodic nanostructures prepared by nano-scale fabrication techniques have the advantages of high uniformity and repeatability, two properties highly favored for chemical sensor applications, plus a moderate SERS enhancement factor ( $10^5$ – $10^6$ ) [21,22]. Since the geometrical textures will change the coupling between the incident light and the SPs, and consequently the amount of SERS enhancement, it is important to study the geometrical tuning effect and optimize the geometrical design for a maximum SERS detection efficiency. The grating structure offers a simple but fascinating system for such a purpose [23,24]. In 2000 the subwavelength dual metallic grating (DMG) structures were proposed by Stephen Chou’s group for planar polarizer applications [25]. The success of these experiments inspired interests in these structures and, consequently, DMG optical properties as well as the surface plasmon behaviors were studied [26–32]. In 1998 Kahl and Voges [33] reported a SERS study on silver DMG structures and suggested that an optimum grating height should be used for reproducible SERS measurements in backscattering geometry [34].

In this work we investigate the SERS enhancement of gold DMG structures for a range of  $\text{SiO}_2$  grating heights and incident polarization angles. An optimum grating height and incident polarization angle are found, giving a large enhancement factor of  $10^5$ . The 2D finite difference time domain (FDTD) simulations reveal that the surface plasmon coupling plays a key role in the SERS enhancement on these DMG structures.

A typical scanning electron microscopy (SEM) image of the DMG structure is shown in Figure 1(a). A schematic plot of the DMG structure is shown in Figure 1(b), where the  $\text{SiO}_2$  grating periodicity  $D$ , grating width  $w$ , grating height  $h_1$  and gold coating layer thickness  $h_2$  are indicated. In this work  $D=400$  nm,  $w=250$  nm, and  $h_2=100$  nm were used, while  $h_1$  ranges from 165 to 550 nm. This grating structure was first transferred to a resist layer on a one-inch Si wafer coated with an 850 nm  $\text{SiO}_2$  layer by nanoimprint lithography, followed by the oxygen plasma treatment to remove the residual scum layer. Next, a layer of Cr was

deposited via thermal evaporation and then the lift-off process was used to produce the Cr etch mask for  $\text{SiO}_2$  reactive ion etching (RIE).  $\text{SiO}_2$  etch depth was controlled by the etching time. The RIE recipe was optimized to obtain nearly vertical sidewalls, which is crucial to limit gold deposition on the sidewalls. After RIE, the Cr layer was removed by wet etching. Finally, gold was thermally evaporated on the  $\text{SiO}_2$  grating surface. The sample surface was placed normal to the gold diffusion path and, thus, only a minimal amount of gold was deposited on the grating sidewalls. Nanoimprint lithography has the advantage of high precision dimension control, high throughput and low cost and, therefore, greatly facilitates the integration of DMG structures into SERS-active substrates.

Benzenethiol (BT) is chosen as the SERS probe molecule due to its large Raman cross section and ability to self-assemble into a dense monolayer on a gold surface. For the sample preparation, the DMG structures were immersed in a 10 mM solution of BT in ethanol for 10 h, rinsed thoroughly with adequate ethanol and then blown dry with nitrogen. This procedure ensures that at most one monolayer of BT is present on the gold surface.

Raman spectra from our samples were collected in the back scattering geometry with a  $50\times$  ( $NA=0.75$ ) objective. Samples were illuminated at normal incidence with a linearly polarized 632.8 nm HeNe laser (12.3 mW). Raman scattered light was routed to a Renishaw inVia Raman system. Polarization of the incident radiation was rotated by passing the laser beam through a half-wave plate prior to entry into the microscope optical path. This arrangement allows the direction of the polarization vector to be rotated with regard to the main axis of the grating structures. The diameter of the laser spot with the  $50\times$  objective is adjusted to 15  $\mu\text{m}$  by passing the beam through a beam expander in order to ensure that at least ten periods of the grating are illuminated. The incident power at the substrate surface was adjusted to less than 1.5 mW in order to avoid thermally ablating the BT molecules during the lengthy acquisition time.

A typical Raman spectrum of the BT molecules adsorbed on a DMG structure is shown in Figure 2(a), for  $h_1=330$  nm,  $p$ -polarized (electric field perpendicular to the main axis of the grating) incident light, and 1 s integration time. The monolayer adsorption of BT molecules on the gold surface

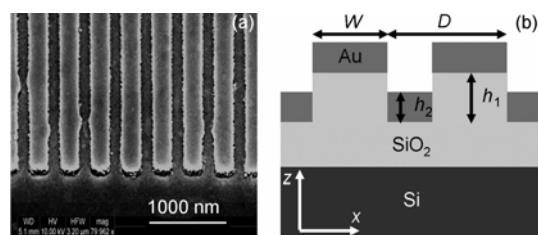


**Figure 1** (a) Tilted SEM image of the gold DMG structure for  $h_1=165$  nm,  $D=400$  nm,  $w=250$  nm, and  $h_2=100$  nm. (b) Schematic plot of the DMG structure.

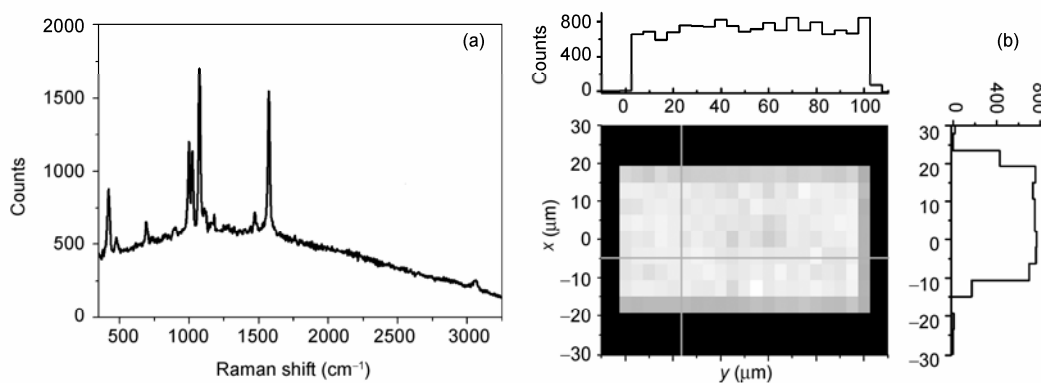


**Figure 2** (a) Typical SERS spectra of BT molecules adsorbed on the DMG structure, for  $h_1=330$  nm,  $p$ -polarized incident light, and an integration time of 1 s. (b) Contour plot of the  $1570\text{ cm}^{-1}$  peak intensity over the sample surface by Raman mapping technique. The bright part corresponds to the grating area. Top and right plots are the Raman intensity scans along  $x$  and  $y$  directions, respectively (indicated by the lines).

was confirmed by the absence of the  $-\text{SH}$  band at  $2600\text{ cm}^{-1}$  in the Raman spectra due to the bonding of sulfur to gold [35]. The spectrum shows a clear and strong Raman signal where the feature peaks coincide with the SERS spectra published [36]. For comparison, the spectra taken on the flat gold surface outside the grating area presented no Raman signal of BT molecules at all (not shown). Therefore, the SERS enhancement is from the DMG structure. The magnitude of the enhancement on the DMG was found to be quite uniform over the entire patterned area. From Raman mapping data of the  $1570\text{ cm}^{-1}$  peak (C–C vibration mode [35]) a standard deviation of less than 20% was found, see Figure 2(b). The bright part in Figure 2(b) represents the 2D contour plot of the  $1570\text{ cm}^{-1}$  peak counts on the grating area ( $100\text{ }\mu\text{m} \times 40\text{ }\mu\text{m}$ ), while the dark parts are outside the grating area. The profiles of the mapping data along the  $x$  and  $y$  directions are also shown in Figure 2(b), with a step size of  $5\text{ }\mu\text{m}$ . Time sequence Raman measurements on the DMG structures were also performed for 2 h illumination and recording data every 5 min. The results (not shown) confirmed the good reproducibility of the SERS enhancement on the DMG structures.

Next, the Raman spectra for the DMG structures with different  $\text{SiO}_2$  grating heights are measured with two incident polarization states:  $s$ -polarized (electric field parallel to the main axis of the grating) and  $p$ -polarized (electric field perpendicular to the main axis of the grating). For  $p$ -polarized incident light, the SERS signal dependence on the grating height is shown in Figure 3(a). The Raman spectra are baseline subtracted and normalized by the laser power and the integration time, and vertically shifted for a clearer plot. For  $s$ -polarized incident light, the Raman signal of the BT molecules is weak for all the grating heights, roughly one to two orders lower than for the  $p$ -polarized incident case. For  $p$ -polarized incident light, the small differences of spectra between  $1150\text{ cm}^{-1}$  and  $1500\text{ cm}^{-1}$  for different heights are possibly due to the different enhancement factors and some contaminations on the grating sur-

face. The SERS enhancement factor dependence on the  $\text{SiO}_2$  grating height and incident polarization is summarized in Figure 3(b) (black and red dots). The experimental enhancement factor  $EF_{\text{exp}}$  is defined as the  $1570\text{ cm}^{-1}$  peak counts per molecule on SERS substrate normalized by peak counts per molecule in solution (no enhancement) and given by [4]

$$EF_{\text{exp}} = \frac{I_{\text{SERS}} / (AR / \sigma)}{I_{\text{bulk}} / (cN_A hA)} = \frac{cN_A \sigma h I_{\text{SERS}}}{RI_{\text{bulk}}}$$

where  $c=5\text{ mol/L}$  is the concentration of solution species,  $N_A$  is Avogadro constant,  $h=20\text{ }\mu\text{m}$  is the effective depth of focus,  $A$  is the illuminated area,  $\sigma=0.37\text{ nm}^2$  is the surface area occupied by single BT molecule [37],  $R=1.5$  is taking the ratio of the gold surface area over the projection area as an estimation and omits the surface roughness influence, and  $I_{\text{SERS}}$  and  $I_{\text{bulk}}$  denote the normalized Raman counts (baseline subtracted) measured on the SERS substrate and in the solution, respectively. Taking the measured data  $I_{\text{bulk}}=31\text{ counts}/(\text{mW}\cdot\text{s})$  and  $I_{\text{SERS}}=645\text{ counts}/(\text{mW}\cdot\text{s})$  for  $h_1=330\text{ nm}$  and  $p$ -polarized incident light, an optimum enhancement factor  $EF_{\text{exp}}=3.1 \times 10^5$  is attained, which is comparable to the enhancement factors reported for other periodic structures [21]. The detailed study of the polarization angle dependence of the  $1570\text{ cm}^{-1}$  Raman peak intensity was done by rotating the half-wave plate and recording the Raman spectrum every  $5^\circ$  of half-wave plate rotation. A  $\cos^2\theta$  dependence is fitted with the measured Raman intensity for all the grating heights (Figure 3(c)), which consists with the fact that only the  $p$ -polarized component of the incident light can excite SPs in grating structures. The remaining weak Raman signal of BT molecules for  $s$ -polarized incident light is likely due to the sidewall roughness of the top gold layer, as shown in Figure 1(a).

A more detailed and quantitative explanation is given by 2D-FDTD simulations that calculate the local electric-field distributions on the grating structure. The model of the DMG structure is demonstrated in Figure 1(b), and simu-

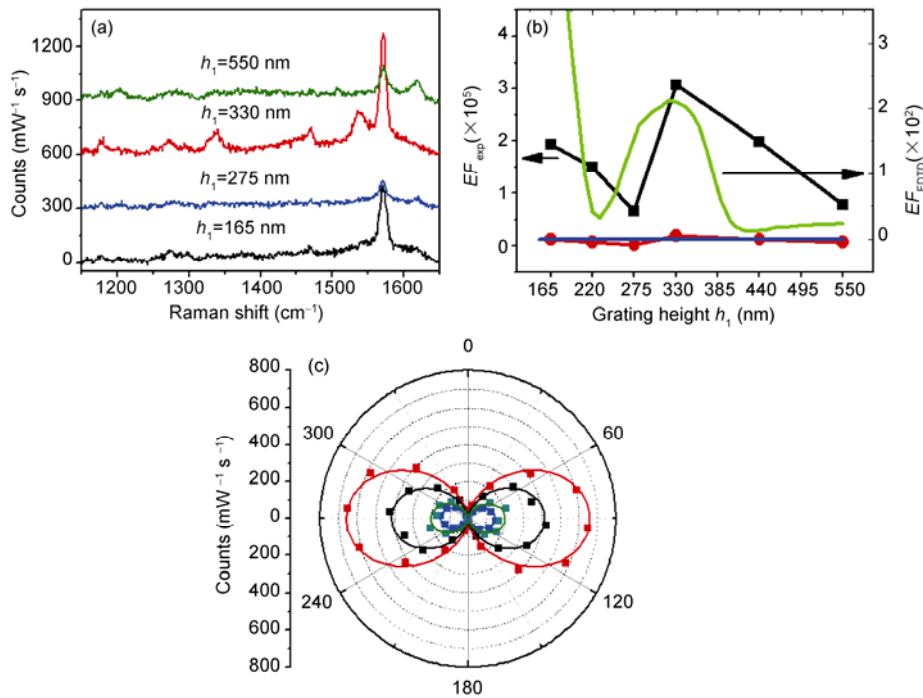


**Figure 3** (a) Raman spectra of BT molecule on DMG structures for  $h_1=165$  nm (black), 275 nm (blue), 330 nm (red) and 550 nm (olive), with baseline subtracted for  $p$ -polarized incident light. (b) Experimental and calculated enhancement factors as a function of SiO<sub>2</sub> grating heights  $h_1$  for  $p$ - and  $s$ -polarized incident light. Red and black dots are experimental values for  $s$ -polarized and  $p$ -polarized incident light, respectively, while the blue and green curves correspond to the FDTD simulation results. (c) 1570 cm<sup>-1</sup> Raman peak intensity as a function of incident polarization angle, baseline subtracted, for the same DMG structures demonstrated in (a). Dots are the measured data, while curves are the  $\cos^2\theta$  fitting.

lated by one periodicity with periodic boundary conditions and a normal incident plane wave source with 633 nm wavelength. The permittivity of gold and the Si substrate are taken from [38] and the refractive index of SiO<sub>2</sub> is taken to be 1.456. The averaged molecular enhancement factor  $EF_{\text{FDTD}}$  is calculated by electro-magnetic field enhancement theory [5] as

$$EF_{\text{FDTD}} = \frac{1}{N_{\text{grid}}} \sum_{m=1}^{N_{\text{grid}}} \frac{|\vec{E}_{s,m}|^2 |\vec{E}_{0,m}|^2}{|\vec{E}_0|^4} \approx \frac{1}{N_{\text{grid}}} \sum_{m=1}^{N_{\text{grid}}} \frac{|\vec{E}_{0,m}|^4}{|\vec{E}_0|^4},$$

which averages the electric field enhancement over the number of grid points,  $N_{\text{grid}}$ , located on top of the gold surface where BT molecules are assumed to reside. The mesh grid size used in the FDTD simulations is 1 nm in length.

The local electric field distributions calculated by FDTD are shown in Figure 4. For  $p$ -polarized incident light, SPs in the gold layers are excited and tuned by the interference of light from top and bottom gold layers. Therefore large electric field enhancement happens for  $h_1=150$  nm (Figure 4(a)) and  $h_1=300$  nm (Figure 4(c)) when SPs of the top gold layer match a constructive interference of light and an enhancement dip appears for  $h_1=220$  nm (Figure 4(b)) when SPs of the top gold layer match a destructive mode. When the grating height is larger than 450 nm, the interference of light from the top and the bottom gold layer is very weak,

and only very weak SPs are excited (Figure 4(d)). For  $s$ -polarized incident radiation, the SPs cannot be excited, explaining why the electric field on the grating surface is quite weak (Figure 4(e) and (f)). The enhancement factor calculated by the 2D FDTD simulations shows similar dependence on the grating height as the experimental data shown in Figure 3(b). The difference to the experimental curve is likely caused by the simple rectangular grating model which ignores the detailed geometric variations [39]. Moreover, the Raman emission cross section on different adsorption sites should be taken into account as well, which could moderate the calculated enhancement with a sharp increase for shallower gratings (the green curve in Figure 3(b)). A further discussion for this will be published later. Notice that the simulated  $EF$  values here are simply due to the excitation of SPs of the gold layers on the DMG structures, and thus the underestimate of three orders of magnitude compared with the experimental data could be due to the omission of the baseline SERS enhancement originating from the sidewall roughness of the gold layers (the red dots in Figure 3(b),  $EF_{\text{exp}} \sim 10^3$ ).

In summary, the SERS enhancement dependence on the grating height and incident polarization is studied for DMG structures. Using  $p$ -polarized incident light and a SiO<sub>2</sub> grating height of  $h_1=330$  nm, an enhancement factor of  $3.1 \times 10^5$  is obtained. Both the  $\cos^2\theta$  dependence of Raman enhancement on incident polarization angle and 2D FDTD simula-

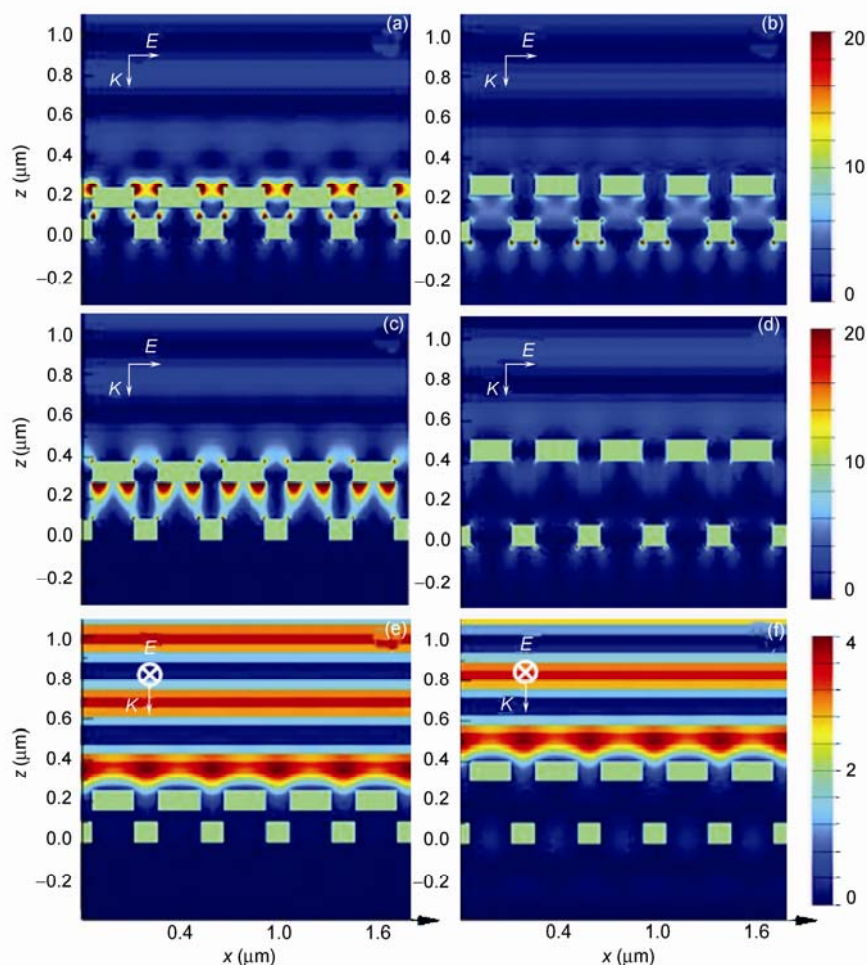


**Figure 4** Calculated electric field intensity distribution,  $|E|$ , in the  $x$ - $z$  plane for DMG structures with  $h_1=150$  nm (a),  $h_1=220$  nm (b),  $h_1=300$  nm (c),  $h_1=410$  nm (d) for  $p$ -polarized incident light, and  $h_1=150$  nm (e),  $h_1=300$  nm (f) for  $s$ -polarized incident light. Green rectangles represent gold layers.

tions confirm that the SPs are responsible for the large local electric field enhancement and consequently the SERS enhancement. This study shows the potential of DMG structures as a highly uniform, reproducible and sensitive SERS substrate.

*This work was supported by the International S&T Cooperation Program of China (2006DFB02020), the National Basic Research Program of China (2007CB936800 and 2009CB930704) and the Hundred Talents Program of the Chinese Academy of Sciences.*

- 1 Moskowitz M. Surface-enhanced spectroscopy. *Rev Mod Phys*, 1985, 57: 783–826
- 2 Otto A. Light Scattering in Solids. Cardona M, Guntherodt G, eds. Berlin: Springer, 1984. 289
- 3 Arya K, Zeyher R. Light Scattering in Solids. Cardona M, Guntherodt G, eds. Berlin: Springer, 1984. 419
- 4 Tian Z Q, Ren B, Wu D Y. Surface-enhanced Raman scattering: From noble to transition metals and from rough surfaces to ordered nanostructures. *J Phys Chem B*, 2002, 106: 9463–9483
- 5 Xu H X, Aizpurua J, Kall M, et al. Electromagnetic contributions to single-molecule sensitivity in surface-enhanced Raman scattering. *Phys Rev E*, 2000, 62: 4318–4324
- 6 Wei H, Hao F, Huang Y Z, et al. Polarization dependence of surface-enhanced Raman scattering in gold nanoparticle-nanowire systems. *Nano Lett*, 2008, 8: 2497–2502
- 7 Yang Z, Wu D, Yao J, et al. SERS mechanism of nickel electrode. *Chinese Sci Bull*, 2002, 47: 1983–1986
- 8 Kneipp K, Wang Y, Kneipp H, et al. Single molecule detection using surface-enhanced Raman scattering (SERS). *Phys Rev Lett*, 1997, 78: 1667–1670
- 9 Xu H X, Bjerneld E J, Kall M, et al. Spectroscopy of single hemoglobin molecules by surface enhanced Raman scattering. *Phys Rev Lett*, 1999, 83: 4357–4360
- 10 Kneipp K, Moskovits M, Kneipp H. *Surface-Enhanced Raman Scattering: Physics and Applications (Topics in Applied Physics)*. New York: Springer, 2006
- 11 Porter M D, Lipert R J, Siperko L M, et al. SERS as a bioassay platform: fundamentals, design, and applications. *Chem Soc Rev*, 2008, 37: 1001–1011
- 12 Chourpa I, Lei F H, Dubois P, et al. Intracellular applications of analytical SERS spectroscopy and multispectral imaging. *Chem Soc Rev*, 2008, 37: 993–1000
- 13 Shafer-Peltier K E, Haynes C L, Glucksberg M R, et al. Toward a glucose biosensor based on surface-enhanced Raman scattering. *J Am Chem Soc*, 2003, 125: 588–593
- 14 Huang X, El-Sayed I H, Qian W, et al. Cancer cells assemble and align gold nanorods conjugated to antibodies to produce highly enhanced, sharp, and polarized surface Raman spectra: A potential cancer diagnostic marker. *Nano Lett*, 2007, 7: 1591–1597

- 15 Qian X, Peng X, Ansari D O, et al. *In vivo* tumor targeting and spectroscopic detection with surface-enhanced Raman nanoparticle tags. *Nat Biotech*, 2008, 26: 83–90
- 16 Wei H, Hakanson U, Yang Z L, et al. Individual nanometer hole-particle pairs for surface-enhanced Raman scattering. *Small*, 2008, 4: 1296–1300
- 17 Bosnick K A, Jiang J, Brus L E. Fluctuations and local symmetry in single-molecule rhodamine 6G Raman scattering on silver nanocrystal aggregates. *J Phys Chem B*, 2002, 106: 8096–8099
- 18 Xu H X, Kall M. Polarization-dependent surface-enhanced Raman spectroscopy of isolated silver nanoaggregates. *ChemPhysChem*, 2003, 4: 1001–1005
- 19 Shegai T, Li Z P, Dadosh T, et al. Managing light polarization via plasmon-molecule interactions within an asymmetric metal nanoparticle trimer. *Proc Natl Acad Sci USA*, 2008, 105: 16448–16453
- 20 Li Z, Shegai T, Haran G, et al. Multiple-particle nanoantennas for enormous enhancement and polarization control of light emission. *ACS Nano*, 2009, 3: 637–642
- 21 Baumberg J J, Kelf T A, Sugawara Y, et al. Angle-resolved surface-enhanced Raman scattering on metallic nanostructured plasmonic crystals. *Nano Lett*, 2005, 5: 2262–2267
- 22 Dick L A, McFarland A D, Haynes C L, et al. Metal film over nanosphere (MFON) electrodes for surface-enhanced Raman spectroscopy (SERS): Improvements in surface nanostructure stability and suppression of irreversible loss. *J Phys Chem B*, 2002, 106: 853–860
- 23 Arnold M, Bussemer P, Hehl K, et al. Enhanced Raman-scattering from benzene condensed on a silver grating. *J Mod Optic*, 1992, 39: 2329–2346
- 24 Baltog I, Primeau N, Reinisch R, et al. Surface-enhanced Raman scattering on silver grating: Optimized antennalike gain of the Stokes signal of  $10^4$ . *Appl Phys Lett*, 1995, 66: 1187–1189
- 25 Yu Z N, Deshpande P, Wu W, et al. Reflective polarizer based on a stacked double-layer subwavelength metal grating structure fabricated using nanoimprint lithography. *Appl Phys Lett*, 2000, 77: 927–929
- 26 Yang Z Y, Zhao M, Dai N L, et al. Broadband polarizers using dual-layer metallic nanowire grids. *IEEE Photonic Tech Lett*, 2008, 20: 697–699
- 27 Cheng C, Chen J, Shi D, et al. Physical mechanism of extraordinary electromagnetic transmission in dual-metallic grating structures. *Phys Rev B*, 2008, 78: 075406
- 28 Cheng C, Chen J, Wu Q, et al. Controllable electromagnetic transmission based on dual-metallic grating structures composed of subwavelength slits. *Appl Phys Lett*, 2007, 91: 111111
- 29 Fong K, Hui P M. Coupling of waveguide and surface modes in enhanced transmission through stacking gratings. *Appl Phys Lett*, 2006, 89: 091101
- 30 Kravets V G, Schedin F, Grigorenko A N. Plasmonic blackbody: Almost complete absorption of light in nanostructured metallic coatings. *Phys Rev B*, 2008, 78: 205405
- 31 Li Q, Jiao X, Wang P, et al. Analysis of novel optical properties of subwavelength double-layer metallic grating. *Appl Phys B*, 2005, 81: 787–790
- 32 Chan H B, Marcet Z, Woo K, et al. Optical transmission through double-layer metallic subwavelength slit arrays. *Opt Lett*, 2006, 31: 516–518
- 33 Kahl M, Voges E, Kostrewa S, et al. Periodically structured metallic substrates for SERS. *Sensor Actuat B*, 1998, 51: 285–291
- 34 Kahl M, Voges E. Analysis of plasmon resonance and surface-enhanced Raman scattering on periodic silver structures. *Phys Rev B*, 2000, 61: 14078–14088
- 35 Szafranski C A, Tanner W, Laibinis P E, et al. Surface-enhanced Raman spectroscopy of aromatic thiols and disulfides on gold electrodes. *Langmuir*, 1998, 14: 3570–3579
- 36 Cintra S, Abdelsalam M E, Bartlett P N, et al. Sculpted substrates for SERS. *Faraday Discuss*, 2006, 132: 191–199
- 37 Liu X F, Sun C H, Linn N C, et al. Wafer-scale surface-enhanced Raman scattering substrates with highly reproducible enhancement. *J Phys Chem C*, 2009, 113: 14804–14811
- 38 Palik E D. *Handbook of Optical Constants of Solids*. San Diego: Academic Press, 1998
- 39 Ekinci Y, Solak H H, David C, et al. Bilayer Al wire-grids as broadband and high-performance polarizers. *Opt Express*, 2006, 14: 2323–2334